RSC Advances

ROYAL SOCIETY OF CHEMISTRY

www.rsc.org/advances

Cite this: DOI: 10.1039/c0xx00000x

www.rsc.org/xxxxxx

ARTICLE TYPE

Hydrothermal assisted sol-gel synthesis and multisite luminescent properties of anatase TiO_2:Eu^{3+} nanorods

Meiqi Chang, Yanhua Song, Hongguang Zhang Ye Sheng, Keyan Zheng, Xiuqing Zhou, Haifeng Zou*

College of Chemistry, Jilin University, Changchun 130012, PR China
Corresponding author Tel.: +86 431 85155275.
E-mail address:zouhf@jlu.edu.cn.

Received (in XXX, XXX) Xth XXXXXXXXX 20XX, Accepted Xth XXXXXXXXX 20XX
DOI: 10.1039/b000000x

Uniform TiO_2:Eu^{3+} spindlelike nanorods have been successfully prepared by a hydrothermal assisted sol-gel process with ethanediamine (ED) as the shape controller. A possible formation mechanism and luminescent properties were investigated by X-Ray diffraction (XRD), scanning electron microscopy (SEM), transmission electron microscopy (TEM), photoluminescence (PL) and kinetic decays. And site-selective spectroscopy was used to research into sites of Eu^{3+} in TiO_2 lattice at 10 K, which identifies two kinds of sites of Eu^{3+} in TiO_2 nanocrystals. One is located in the distorted lattice sites near the surface, and the other is situated in lattice sites with ordered crystalline environment. Moreover, the luminescence decay curve of products further proved the existence of multiple sites of Eu^{3+} ions in TiO_2 nanocrystals.

1. Introduction

Over the past decade, titanium dioxide (TiO_2) has attracted considerable attention due to its widespread applications in fields such as photocatalysis,[1, 2 3] dye-sensitized solar cells,[4, 5] sensors,[6] especially used as luminescence materials.[7-9] Because of unique optical, electrical, and photochemical properties of titania come from its own energy band gap characteristics,[10] TiO_2 is suggested to be a promising host lattice for the luminescence of various optically active lanthanide ions. As we know, the properties of titania are strongly dependent on the morphology and crystallite size. Hence, much more efforts should be made to precisely control crystallinity and morphological features of titania.

Compared with other 1D nanostructures, nanorods with high aspect ratios have become the focus of scientists because of their potential applications in photoelectrochemical hydrogen production,[11] hybrid ultraviolet photodetectors,[12] optical materials,[13] magnetic properties,[14] planar device applications.[15] Titanium oxide nanorods, up to now, have been produced using chemistry methods including hydrothermal routes,[16, 17] self-assembly methods,[18] sol-gel processes,[19] solvothermal methods,[20, 21] and so on. For example, Jiu et al. described that highly crystalline TiO_2 nanorods have been synthesized by a hydrothermal process in a cetyltrimethylammonium bromide surfactant solution.[22] Koo et al have reported the simultaneous phase- and size-controlled synthesis of TiO_2 nanorods were performed via the non-hydrolytic sol-gel method.[23] However, few studies have been reported on the synthesis and the luminescence properties of rare-earth doped TiO_2 nanorods, particularly the luminescence characteristics of multiple sites of Eu^{3+} ions in TiO_2 nanocrystals.

In this article, TiO_2:Eu^{3+} spindlelike nanorods with uniform crystallinity and narrow size distribution have been formed through hydrothermal assisted sol-gel process, which combines the advantages of sol-gel route and hydrothermal method, such as lower reaction temperature, controllable morphology, narrow particle size distribution. The influences of preparation conditions on the crystal phase, crystal shape, as well as the luminescent properties were investigated. Ethanediamine was added to act as a shape controller because it's specifically adsorbed onto the planes parallel to the c-axis of nanoparticles. The formation mechanism of the products was proposed. Furthermore, through site-selective spectroscopy at 10 K, we have found two kinds of sites of Eu^{3+} ions with different luminescent characteristics doped in TiO_2 nanocrystals.

2. Experimental

2.1 Materials

Tetrabutyl titanate, triethanolamine, ethylenediamine, absolute ethanol and Eu_2O_3 (99.99%) were purchased from Beijing Chemical Co.All chemicals were analytical-grade reagents and used directly without further purification. The $Eu(NO_3)_3$ aqueous solution was obtained by dissolving Eu_2O_3 (99.99%) in dilute HNO_3 solution under heating with vigorously agitation. Deionized water was used for all treatment processes.

2.2 Synthesis of the TiO_2:Eu^{3+} nanorods

In this article, tetrabutyl titanate (TBOT) was chosen as titanium source. Firstly, TBOT and triethanolamine (TEOA) were mixed with a molar radio of [TBOT]:[TEOA] = 1:2 to form a stable compound of Ti^{4+} in order to avoid rapid hydrolysis of Ti^{4+}, and then the molar concentration of Ti^{4+} reached to 0.5 mol/L by the addition of deionized water. The stock solution was mixed with the same volume of aqueous solution of ethylenediamine (0.6 mol/L) with magnetic stirring. Then 0.2 mL $Eu(NO_3)_3$ (0.5 mol/L) was added to above solution. The final solution was transferred into a Teflon stainless steel autoclave aged at 100 ℃ for 24 h for gelation (the first aging), and further aged at 140 ℃ for 72 h to achieve the nucleation and growth of titania (the second aging). The autoclave was then cooled to room temperature naturally. Finally, the white precipitate was washed with deionized water and absolute ethanol several times. The products were dried at 60 ℃ for 12 h in air.

2.3 Characterization

The crystalline phase of the TiO_2:Eu^{3+} nanorods were distinguished by standard X-ray diffraction (XRD) (Rigaku D/max-B II) with Cu-Kα radiation (λ = 0.15405 nm) over a 2θ range from 10° to 70°. The morphology of the products was inspected using a scanning electron microscope (S-4800, Hitachi) and transmission electron microscopy (FEI Tecnai G^2S-Twin) with a field-emission gun operating at 200 kV. Photoluminescence excitation and emission spectra were recorded with a Jobin Yvon FluoroMax-4 equipped with a 150 W xenon lamp as the excitation source. For low temperature measurement, the samples were mounted in the helium-exchange gas chamber of a closed-cycle refrigeration system, and their temperature was maintained at 10 K. A Rhodamine 6G dye laser pumped by the second harmonic of an Nd:yttrium–aluminum–garnet pulsed laser was used as the excitation source. The site-selective spectra were obtained with a Spex 1403 spectrometer. The photoluminescence signals were detected with a photomultiplier, averaged with a boxcar integrator, and processed by a computer.

3. Results and discussion

3.1 Crystal Structure and phase composition

As is known to all, TiO_2 exists in three mineral forms: anatase (tetragonal), rutile (tetragonal) and brookite (orthorhombic).[24] Generally, TiO_2 is preferred in anatase form with wide band gap (3.2 eV) and higher electron mobility. In this article, X-ray diffraction (XRD) analyses were performed to investigate the phase and purity of the products. As illustrated in Figure 1, all diffraction peaks match well with the crystal structure of the anatase TiO_2 (JCPDS No.21-1272), and no additional peaks for others phases have been found, which indicates that Eu^{3+} ions have been built into the TiO_2 host lattice effectively. The main diffraction peaks may shift slightly because of the different radius between Eu^{3+} ions and Ti^{4+} ions. However, the shift of diffraction peaks has not been detected in our experiments due to the low doping concentrating of Eu^{3+} ions. The energy dispersive X-ray (EDX) spectrum was further used to analyse the composites of the as-obtained TiO_2:Eu^{3+} nanorods, as shown in Figure 2. The result confirms the presence of Ti, O, and Eu elements in the products, which is in agreement with the XRD result above.

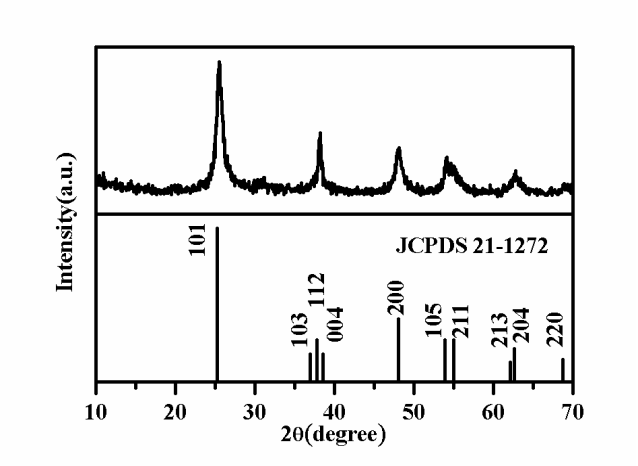

Figure 1. XRD patterns of the as-synthesized TiO_2:Eu^{3+} nanorods, along with the standard data for the anatase TiO_2 (JCPDS card 21-1272) as references.

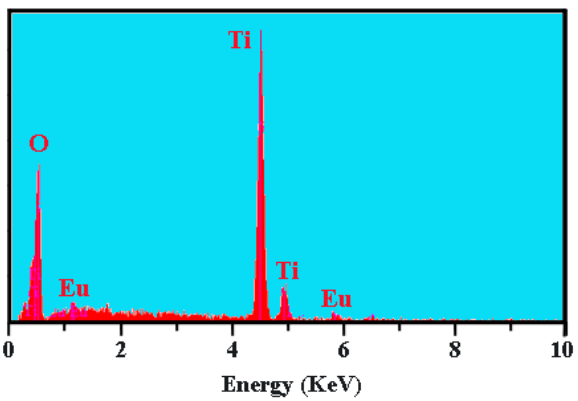

Figure 2. EDX spectrum of the TiO_2:Eu^{3+} nanorods.

3.2. Morphology

The morphology and microstructure details of the as-prepared nanorods were surveyed by means of SEM and TEM. Figure 3a shows the SEM image of Eu^{3+} doped titania nanorods. It can be seen that the sample is composed of the uniform spindle-shape nanorods. To further study the texture of the products, a TEM micrograph (Figure 3b) for the as-prepared sample clearly shows the obvious spindlelike nanorods with an average size of 45 nm in width and 500 nm in length, which is in consistent with the SEM result.

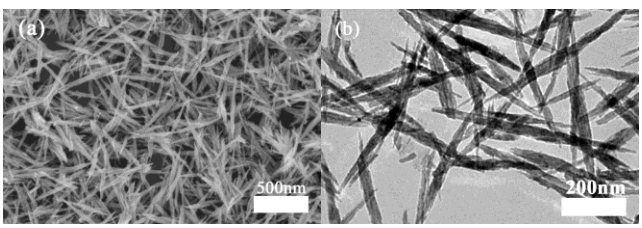

Figure 3. (a) SEM, and (b) TEM images of TiO_2:Eu^{3+} spindlelike nanorods.

3.3. Effect of the dosage of the shape controller

Many 1D compound nanostructures were obtained with the assistant of additives. As a shape controller, ethanediamine played an important role in the synthesis of TiO_2:Eu^{3+} spindlelike nanorods for its complete growth. And the reaction time is 96 h. As shown in Figure 4, different dosages of ED were added to understand its effect on the growth of TiO_2:Eu^{3+} nanocrystals. When ED was absent in the raw materials while other conditions remained the same, the products were composed of uniform ellipsoidal nanoparticles with lower aspect ratio (Figure 4a). When the dosage of ED rose to 0.2 mol/L and 0.4 mol/L (Figure 4b, and 4c), some imperfect spindlelike nanorods formed by aggregation of the smaller nanoparticles which have already formed. And the monodisperse and uniform nanoparticles with higher aspect ratio have been achieved when the amount of ED is 0.6 mol/L (Figure 4d). As the amount of ED further increased to 0.8 mol/L and 1.0 mol/L (Figure 4e, and 4f), a large number of nanoparticles aggregated together with no definite shape. In this work, ED plays a decisive role to produce the uniform spindlelike nanostructure (i) as a shape controller by adsorbing onto the planes parallel to the c-axis of nanoparticles and (ii) as a capping agent to balance the growth rates of different facets.

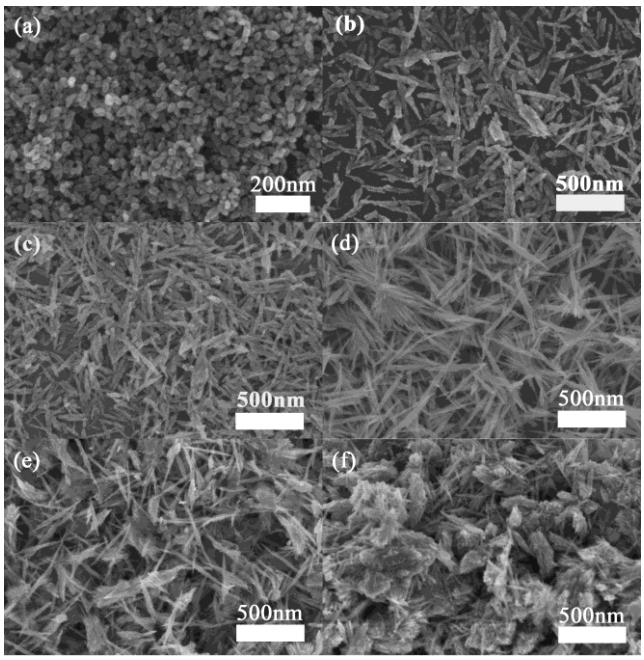

Figure 4. SEM images of the TiO_2:Eu^{3+} spindlelike nanorods with different dosages of ED: (a) 0, (b) 0.2, (c) 0.4, (d) 0.6, (e) 0.8, and (f) 1.0 mol/L.

3.4. Effect of reaction time

In order to investigate the growth mechanism of the TiO_2:Eu^{3+} spindlelike nanorods, the SEM images of the products obtained at different time intervals are shown in Figure 5. And you can notice that when the dosage of ED rose to 0.6 mol/L, uniform spindlelike nanoparticles were formed from Figure 4. So this dosage has been selected for optimizing the time. When the reaction time was 36 h and 48 h (Figure 5a and 5b), no definite shape was obtained. With the extension of the reaction time (Figure 5c-5e), more and more spindle-shaped nanorods appeared. Until the reaction time was increased to 96 h, the final products were uniform and monodispersed spindlelike nanorods (Figure 5f).

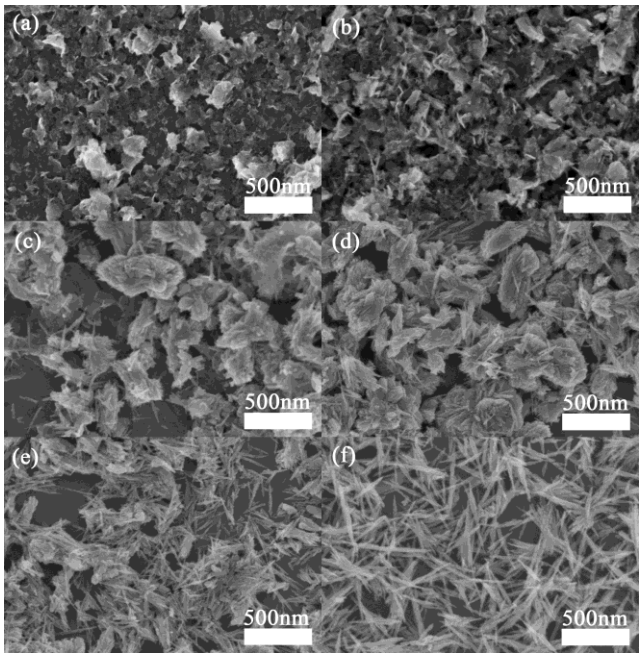

Figure 5. SEM images of the TiO_2:Eu^{3+} nanorods obtained after the reaction proceeded for (a) 36, (b) 48, (c) 60, (d) 72, (e) 84 (f) 96 h.

3.5. Formation mechanism

According to the above experimental results, a possible formation mechanism of the spindlelike TiO_2:Eu^{3+} nanorods is illustrated in Figure 6. The formation process includes chelation, gelation, nucleation and growth stage. Firstly, the stable complex formed through reaction of tetrabutyl titanate (TBOT) and triethanolamine (TEOA), TEOA plays the role of a stabilizer of Ti (IV) ions against its rapid hydrolysis to $Ti(OH)_4$ in the alkaline range.[25-27] The first aging at 100 ℃ for 24 h in autoclave provides a high temperature and high pressure environment, so the chelating ability of the stable complex would become weaker. Almost all TEOA molecules were found to be liberated after the hydrolysis of Ti^{4+} ions, then the $Ti(OH)_4$ gel formed. The gel network acts as a reservoir of the Ti^{4+} ions to reduce the excessive supersaturation leading to extensive nucleation during their growth and as an anticoagulant fixing the growing nanoparticles in the matrix, which plays a decisive role to produce the monodisperse titania nanoparticles. After the dissolution of the $Ti(OH)_4$ gel, the nucleation and growth of TiO_2 happened at 140 ℃ for 72 h in the second aging process. As the shape controller, ED adsorbed selectively onto the different crystal facets of the growing nanoparticles and changed the relative surface energy of different crystal facets, and brought about an effect on the growth rates along certain orientations. In our research, ED specifically adsorbed onto the planes parallel to the c-axis, so these crystal nuclei aggregated to grow along this direction simultaneously and formed spindle-shaped nanorods. Therefore, in the presence of ED, the nanoparticles finally form uniform TiO_2:Eu^{3+} spindlelike nanorods.

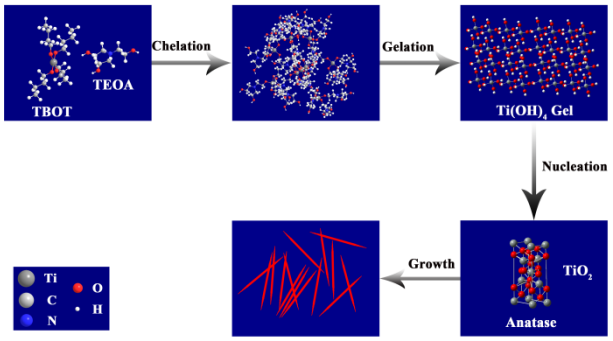

Figure 6. Formation mechanism of the TiO_2:Eu^{3+} spindlelike nanorods.

3.5. Luminescence Properties

Figure 7 shows the excitation and emission spectra of the as-prepared TiO_2:Eu^{3+} spindlelike nanorods at room temperature. The excitation spectrum was obtained by monitoring the emission of the Eu^{3+} ions $^5D_0$-$^7F_2$ transition at 612 nm (Figure 7a). The excitation spectrum consists of Eu^{3+} ions characteristic excitation peaks (382, 393, 414, 464, and 525 (533) nm), which are due to the f-f transition of Eu^{3+} ions from the $^7F_0$ to $^5G_2$, $^5L_6$, $^5D_3$, $^5D_2$ and $^5D_1$ levels. Upon excitation at 393 nm, the emission spectrum exhibits five groups of emission lines (577, 590 (596), 612, 651 and 685 (703) nm), which are ascribed to the $^5D_0$-^7F_J (J = 0, 1, 2, 3, 4) transitions of the Eu^{3+} ions, respectively. The major emissions are 590 nm ($^5D_0$-$^7F_1$) and 612 nm ($^5D_0$-$^7F_2$) correspond to the magnetic dipole transition and electric dipole transition. The Eu^{3+} ions can be used as a probe for the crystal field environments through comparison of the intensity of the $^5D_0$-$^7F_1$ (590 nm) transition with that of the $^5D_0$-$^7F_2$ (612 nm) transition. As shown in Figure 7b, the electric dipole transition is much stronger than the magnetic dipole transition, so the emission spectrum is dominated by the $^5D_0$-$^7F_2$ (612 nm) transition of the Eu^{3+} ions which is hypersensitive to the environment.[28] It suggests that Eu^{3+} ions occupy low-symmetry sites without an inversion center.[29-31] The site symmetries for the Ti^{4+} ions are D_{2d} in anatase lattice. According to the branching rules of the 32 point groups, because of a large mismatch in ionic radius and the charge imbalance between Ti^{4+} and Eu^{3+}, the substitution of the Ti^{4+} with Eu^{3+} ions created oxygen vacancies and caused the lattice distortion, which makes a descent of the D_{2d} to lower site symmetry.

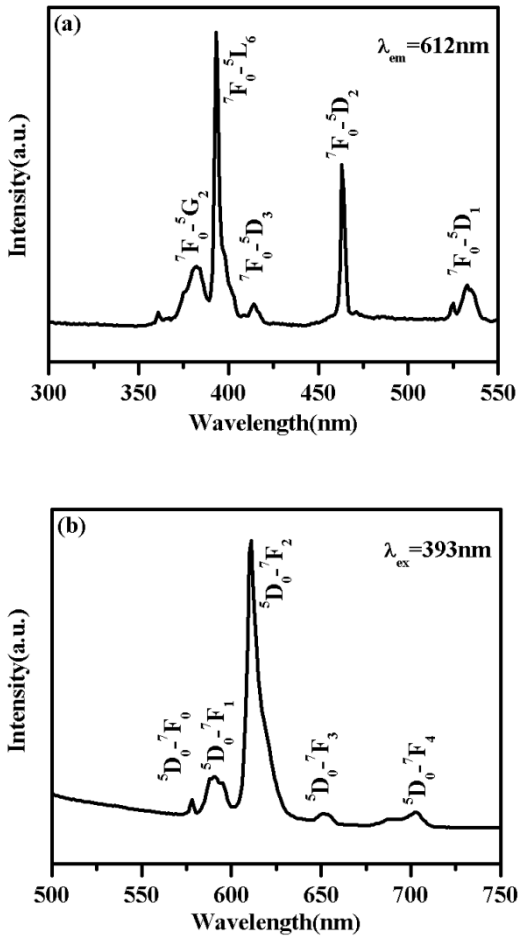

Figure 7. (a) Excitation and (b) emission spectra of the TiO_2:Eu^{3+} spindlelike nanorods.

Site-selective spectroscopy at 10 K were performed to research into doped positions of Eu^{3+} ions in TiO_2 nanocrystals using the experience of Chen et al.[32] for reference. As shown in Figure 8, under excitation at 464.6 nm, we can see that electric dipole transition (614 nm) is much stronger than magnetic dipole transition (590 nm), suggesting that Eu^{3+} ions occupy low-symmetry sites without an inversion center, which has further proved that Eu^{3+} ions have doped in the distorted lattice sites near the surface. However, under excitation at 470.7 nm and 472.1 nm, the magnetic dipole transition intensity is stronger than the electric dipole transition intensity, indicating that the Eu^{3+} ions may occupy the C_{2v}, D_2 high symmetry sites with an inversion center[33] in tetragonal anatase TiO_2, which can interpret that Eu^{3+} ions have doped in lattice sites with ordered crystalline environment. G. K. Liu.et.al. have discussed the mechanisms for anomalous luminescence properties of Eu^{3+} ions at two main sites of BaFCl microcrystals through charge transfer vibronic exciton(CTVE) model.[34] In this article, CTVE model and oxygen vacancy can be used to interpret the multisite structure of Eu^{3+} in anatase nanocrystals. The C_{2v} symmetry site is formed because of lattice uniform relaxation at different directions and the formation of oxygen vacancy. However, for D_2 symmetry site, the oxygen vacancy is not completely formed, instead, the charge transfer vibronic exciton has been formed to compensate for the charge

imbalance and lattice uneven expansion at different directions.

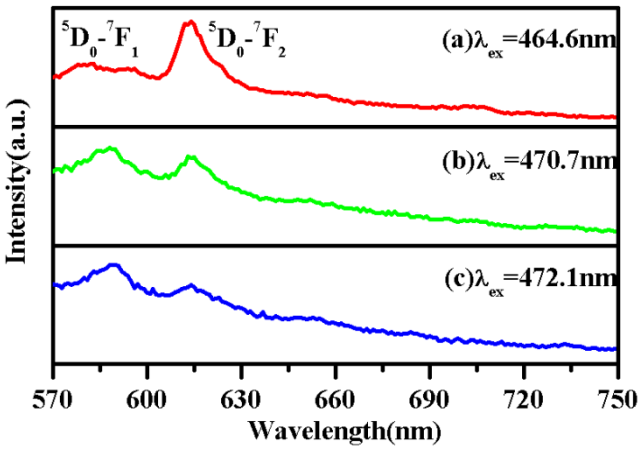

Figure 8. 10 K emission spectra of TiO_2:Eu^{3+} nanorods with λ_{ex} = (a) 464.6, (b) 470.7, and (c) 472.1 nm. The nanorods were excited with a xenon lamp at 464–472 nm under the same experimental condition. To eliminate the influence of excitation light, a 495 nm long-pass glass filter was used.

To further confirm the multiple sites of Eu^{3+} ions doped in TiO_2 crystalline host lattice, decay curve of the $^5D_0$-$^7F_2$ transition of the Eu^{3+} (λ_{em} = 612 nm) in the TiO_2:Eu^{3+} nanorods was determined, which can provide dynamics evidence for the different multiple sites. As shown in Figure 9, the curve cannot be fitted into the single-exponential function but can be fitted well into a double-exponential function as $I = A_1 \exp(-t/\tau_1) + A_2 \exp(-t/\tau_2)$, in which A_i (i = 1, 2) is a pre-exponential factor obtained from the curve fitting, and τ_i (i = 1, 2) is the decay lifetime. The PL lifetimes for the $^5D_0$ state of the Eu^{3+} ions in the TiO_2 nanorods are 0.563 ms and 0.106 ms, corresponding to Eu^{3+} ions ordered lattice sites and distorted lattice sites near the surface, respectively. However, we have noticed that decay time in the distorted lattice sites becomes short due to the quenching effect of the surface defects which come from surface states of TiO_2:Eu^{3+} nanorods.[35] When the excited luminescent centers are near quenching centers which exist in the products, the excited energy will be tranferred to these quenching centers, leading to the shorter lifetime.

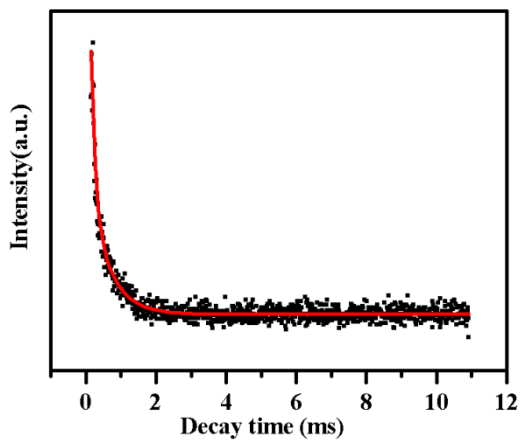

Figure 9. Decay curve for the $^5D_0$-$^7F_2$ (612 nm) emission of the Eu^{3+} ions in TiO_2:Eu^{3+} nanorods.

Conclusions

In summary, a hydrothermal assisted sol-gel process has been introduced to incorporate Eu^{3+} ions into TiO_2 spindlelike nanorods. Ethanediamine acted as a shape controller and specifically adsorbed onto the planes parallel to the c-axis of the TiO_2 nanoparticles. The possible formation mechanism includes chelation, gelation, nucleation and growth stage has been discussed in detail. Most importantly, we have confirmed that the multiple sites structure of Eu^{3+} ions doped in TiO_2 through site-selective spectroscopy at 10 K. Using Eu^{3+} as an optical probe, the relationship between local structure of Eu^{3+} ions and luminescence properties was discussed. We have found two kinds of sites of Eu^{3+} in TiO_2 nanocrystals, one is in the distorted lattice sites near the surface, and the other is lattice sites with ordered crystalline environment. And the decay curve has further proved this point. Furthermore, the TiO_2:Eu^{3+} spindlelike nanorods without any calcination treatment exhibit bright red ($^5D_0$-$^7F_2$) luminescence under ultraviolet excitation. Owing to the uniform sizes and favorable luminescent properties of the products, TiO_2:Eu^{3+} nanorods possess a prosperous application in the fields of optics and electronics in the future.

Acknowledgements

This work was financially supported by the National Natural Science Foundation of China (Grant Nos. 21171066 and 51272085).

Note and references

1. K. Hashimoto, H. Irie and A. Fujishima, *Japanese journal of applied physics*, 2005, **44**, 8269.
2. R. Asahi, T. Morikawa, H. Irie and T. Ohwaki, *Chemical reviews*, 2014, **114**, 9824-9852.
3. S. Manu and M. A. Khadar, *Journal of Materials Chemistry C*, 2015.
4. D. Chen, F. Huang, Y. B. Cheng and R. A. Caruso, *Advanced Materials*, 2009, **21**, 2206-2210.
5. S.-I. In, K. P. Almtoft, H. Lee, I. H. Andersen, D. Qin, N. Bao and C. Grimes, *Bull. Korean Chem. Soc*, 2012, **33**, 1989.
6. J.-C. Xu, W.-M. Liu and H.-L. Li, *Materials Science and Engineering: C*, 2005, **25**, 444-447.
7. H. Zhang, Y. Sheng, K. Zheng, X. Zhou, Z. Shi, X. Xu and H. Zou, *European Journal of Inorganic Chemistry*, 2014, **2014**, 3305-3311.
8. J.-G. Li, X. Wang, K. Watanabe and T. Ishigaki, *The Journal of Physical Chemistry B*, 2006, **110**, 1121-1127.

9. M. Pal, U. Pal, J. M. G. Y. Jiménez and F. Pérez-Rodríguez, *Nanoscale research letters*, 2012, **7**, 1-12.
10. Y.-M. Sung and J.-K. Lee, *Crystal growth & design*, 2004, **4**, 737-742.
11. I. S. Cho, Z. Chen, A. J. Forman, D. R. Kim, P. M. Rao, T. F. Jaramillo and X. Zheng, *Nano letters*, 2011, **11**, 4978-4984.
12. Y. Han, L. Wu, H. Gu, H. Chen and Z. Zhang, *Journal of Materials Science: Materials in Electronics*, 2013, **24**, 1220-1224.
13. N. Kiomarsipour and R. S. Razavi, *Ceramics International*, 2013, **39**, 813-818.
14. S. Wu, Y. Lv, M. Lu and Z. Lin, *Journal of Materials Chemistry C*, 2015, **3**, 3121-3127.
15. D. Singh, A. Narasimulu, L. Garcia-Gancedo, Y. Fu, T. Hasan, S. Lin, J. Geng, G. Shao and J. Luo, *Journal of Materials Chemistry C*, 2013, **1**, 2525-2528.
16. B. Liu and E. S. Aydil, *Journal of the American Chemical Society*, 2009, **131**, 3985-3990.
17. Y. V. Kolen'ko, K. A. Kovnir, A. I. Gavrilov, A. V. Garshev, J. Frantti, O. I. Lebedev, B. R. Churagulov, G. Van Tendeloo and M. Yoshimura, *The Journal of Physical Chemistry B*, 2006, **110**, 4030-4038.
18. J. Liu, H. Bai, Y. Wang, Z. Liu, X. Zhang and D. D. Sun, *Advanced Functional Materials*, 2010, **20**, 4175-4181.
19. J. Joo, S. G. Kwon, T. Yu, M. Cho, J. Lee, J. Yoon and T. Hyeon, *The Journal of Physical Chemistry B*, 2005, **109**, 15297-15302.
20. L. Liu, Y. Zhao, H. Liu, H.-Z. Kou and Y. Wang, *Nanotechnology*, 2006, **17**, 5046.
21. Z. He, J. Liu, J. Miao, B. Liu and T. T. Y. Tan, *Journal of Materials Chemistry C*, 2014, **2**, 1381-1385.
22. J. Jiu, S. Isoda, F. Wang and M. Adachi, *The Journal of Physical Chemistry B*, 2006, **110**, 2087-2092.
23. B. Koo, J. Park, Y. Kim, S.-H. Choi, Y.-E. Sung and T. Hyeon, *The Journal of Physical Chemistry B*, 2006, **110**, 24318-24323.
24. K. Manjumol, M. Jayasankar, K. Vidya, A. P. Mohamed, B. N. Nair and K. Warrier, *Journal of Sol-Gel Science and Technology*, 2015, **73**, 161-170.
25. J.-W. Shiu, C.-M. Lan, Y.-C. Chang, H.-P. Wu, W.-K. Huang and E. W.-G. Diau, *ACS nano*, 2012, **6**, 10862-10873.
26. T.-T. Li, S. Cao, C. Yang, Y. Chen, X.-J. Lv and W.-F. Fu, *Inorganic chemistry*, 2015, **54**, 3061-3067.
27. K. Nakagawa, T. Jia, W. Zheng, S. M. Fairclough, M. Katoh, S. Sugiyama and S. C. E. Tsang, *Chemical Communications*, 2014, **50**, 13702-13705.
28. S. Prashantha, B. Lakshminarasappa and B. Nagabhushana, *Journal of Alloys and Compounds*, 2011, **509**, 10185-10189.
29. L. Żur, J. Janek, M. Sołtys, J. Pisarska and W. Pisarski, *Physica Scripta*, 2013, **2013**, 014035.
30. B. Judd, *Physical Review*, 1962, **127**, 750.
31. J. Liao, B. Qiu, H.-R. Wen, Y. Li, R. Hong and H. You, *Journal of materials science*, 2011, **46**, 1184-1189.
32. X. Chen and W. Luo, *Journal of nanoscience and nanotechnology*, 2010, **10**, 1482-1494.
33. G. Ju, Y. Hu, L. Chen, X. Wang, Z. Mu, H. Wu and F. Kang, *Optics & Laser Technology*, 2012, **44**, 39-42.
34. X. Chen, W. Zhao, R. Cook and G. Liu, *Physical Review B*, 2004, **70**, 205122.
35. Y. Zheng, H. You, G. Jia, K. Liu, Y. Song, M. Yang and H. Zhang, *Crystal Growth & Design*, 2009, **9**, 5101-5107.

Hydrothermal assisted sol-gel synthesis and multisite luminescent properties of anatase $TiO_2:Eu^{3+}$ nanorods

Meiqi Chang, Yanhua Song, Hongguang Zhang Ye Sheng, Keyan Zheng, Xiuqing Zhou, Haifeng Zou*

College of Chemistry, Jilin University, Changchun 130012, PR China
Corresponding author Tel.: +86 431 85155275.
E-mail address:zouhf@jlu.edu.cn.

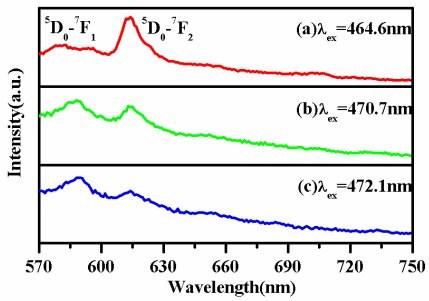

The relationship between local structure of Eu^{3+} ions and luminescence properties were discussed through site-selective spectroscopy at 10 K.